ORIGINAL ARTICLE

Rabies virus infection and immune activation in human epidermal keratinocytes: Implications for rabies transmission

Keshia Kroh[1], Alisha D. Biharie[1], Eleanor M. Marshall[1], Redwan Rahmat[1], Debby Schipper[1], Leanne C. Helgers[2,3], Teunis B.H. Geijtenbeek[2,3], Corine H. GeurtsvanKessel[1] and Carmen W.E. Embregts[1]

Journal of Investigative Dermatology (2026) ■, ■–■; doi:10.1016/j.jid.2026.01.036

Rabies is a fatal zoonotic infection caused by rabies virus (RABV), which is transmitted through the saliva of infected animals. Although most cases are caused by dog bites, superficial exposures such as bat bites or scratches can also lead to infection, although the underlying mechanisms remain poorly understood. We recently detected RABV-positive keratinocytes in skin samples of experimentally infected mice and naturally infected dogs, prompting us to investigate their role in rabies pathogenesis and the antiviral immune response. We confirmed that both the keratinocyte cell line HaCaT and primary keratinocytes are susceptible to RABV infection in vitro, with higher infection rates observed for the attenuated SAD P5/88 Potsdam and silver-haired bat RABV strains than for a dog-related strain. Keratinocytes showed a significant immune activation in response to these 2 strains, as measured by expression of relevant surface markers and cytokine release. To explore whether RABV can be transmitted from infected keratinocytes to neurons, we developed a coculture model using HaCaT and a neuronal cell line separated by a microporous membrane. Virus transfer to the neurons was observed while the barrier integrity remained intact, suggesting that keratinocytes may contribute to RABV transmission and neuroinvasion after superficial exposure.

Keywords: Antiviral response, Barrier immunity, Infectious diseases, Neuroinvasion, Rabies virus

INTRODUCTION

Rabies is a neglected tropical disease, responsible for at least 59,000 human deaths per year (Hampson et al, 2015). Over 99% of human cases result from transmission of rabies virus (RABV) through the saliva of infected dogs (Fooks et al, 2017). The bites of rabid dogs typically cause significant tissue damage down to the muscle, and the virus is thought to enter the nervous system through the neuromuscular junction (Hemachudha et al, 2013). As dog vaccination programs become increasingly effective, other host species, particularly bats, are gaining importance in human rabies transmission. In the United States, for example, 70% of human rabies cases between 1960 and 2018 were in fact attributed to contact with bats (Pieracci et al, 2019).

Unlike dog bites, bat bites or scratches typically do not penetrate deeply enough to reach muscle tissue and the innervating motor neurons, instead they deposit the virus in more superficial layers such as the dermis or epidermis (Begeman et al, 2018). Entry of RABV particles into the nervous system is crucial for the development of rabies disease, eventually causing death due to viral encephalitis and a progressive neuronal dysfunction (Fooks et al, 2017). The dermis and epidermis are rich in sensory nerve endings, providing a potential entry route for RABV (Begeman et al, 2018; Ständer and Schmelz, 2024). The possibility of contracting rabies through superficial exposures, that is, exposures that do not penetrate beyond the skin layer, is documented not only for bats but also for other domestic and wild animals—such as dogs, cats, or wolves—through scratches, superficial bites, or licks on broken skin (Bharti et al, 2017; Guo et al, 2018; Simani et al, 2012). This is reflected in current World Health Organization guidelines, which also recommend postexposure prophylaxis for superficial exposures (WHO, 2018). However, the actual risk of contracting rabies through superficial contact and the precise route through which the virus reaches the CNS remain unclear.

Both superficial exposures and deep bites are likely to bring RABV in contact with keratinocytes, which form the epidermis, the outermost layer of the skin. Our group has previously demonstrated the presence of RABV-positive keratinocytes at the site of initial exposure in naturally and

[1]*Department of Viroscience, Erasmus Medical Centre, Rotterdam, The Netherlands;* [2]*Department of Experimental Immunology, Amsterdam UMC, University of Amsterdam, Amsterdam, The Netherlands; and* [3]*Amsterdam Institute for Infection & Immunity, Amsterdam UMC, University of Amsterdam, Amsterdam, The Netherlands*

Correspondence: Carmen W. E. Embregts, Department of Viroscience, Erasmus Medical Centre, Wytemaweg 80, Rotterdam 3015CN, The Netherlands. E-mail: c.embregts@erasmusmc.nl

Abbreviations: dogRV, dog-related rabies virus; HPEK, human primary epidermal keratinocyte; MOI, multiplicity of infection; RABV, rabies virus; RABV-N, rabies virus nucleoprotein; SHBRV, silver-haired bat rabies virus; TEER, transepithelial electrical resistance

Received 4 September 2025; revised 21 November 2025; accepted 20 January 2026; accepted manuscript published online XXX; corrected proof published online XXX

experimentally infected animals (Kroh et al, 2025a). Although infection after superficial RABV inoculation of the ear skin could not be confirmed in mice experimentally, the findings raised important questions regarding the role of keratinocytes in RABV pathogenesis. Therefore, in this study, we aimed to characterize RABV infection of keratinocytes in vitro, using the human keratinocyte cell line HaCaT and human primary epidermal keratinocytes (HPEKs). Prior studies suggest that RABV strains associated with dogs or bats differ in their tropism, potentially owing to differences in exposure routes (Morimoto et al, 1996; Murphy et al, 1973). Therefore, we chose to compare 2 pathogenic street virus strains: silver-haired bat RABV (SHBRV) and a dog-related RABV (dogRV) strain. In addition, we included the attenuated vaccine strain SAD P5/88 Potsdam (denoted as SAD P5).

RABV employs several immune evasion mechanisms, often preventing sufficient immune cell activation and the generation of virus-neutralizing antibodies in natural infections, likely contributing to its nearly 100% fatality rate (Fooks et al, 2017; Katz et al, 2017). However, keratinocytes are known for their intrinsic immune responses, including cytokine production, antigen presentation, and immune cell recruitment, which enable them to participate in pathogen recognition and the initiation of immune responses (Jiang et al, 2020; Wang and Li, 2020). To investigate whether RABV can activate keratinocytes, we examined the response of human keratinocytes to RABV exposure in vitro. For several cutaneously transmitted viruses, including herpes simplex virus type 2 and dengue virus, keratinocytes have been shown to contribute to antiviral defense by producing cytokines and activating immune cells (Duangkhae et al, 2018; Shao et al, 2010). In this study, we assessed the upregulation of immune-related surface markers ICAM-1, which mediates immune cell recruitment; HLA-DR and HLA-ABC, which are critical for antigen presentation; and PD-L1, a coinhibitory molecule involved in immune regulation (Black et al, 2007; Kroh et al, 2024; Okiyama and Katz, 2014). In addition, we quantified the secretion of antiviral cytokines after RABV exposure to assess the extent of keratinocyte activation.

In healthy skin, sensory nerve endings extend into the epidermis, where they detect tactile stimuli, temperature changes, pain, and itch (Ständer and Schmelz, 2024). These nerve fibers are in close anatomical and functional contact with keratinocytes, engaging in bidirectional communication that modulates the activity of both cell types. This interaction is mediated through the release of neurotransmitters, neuropeptides, and neuronal GFs as well as through direct signal transduction mechanisms (Ständer and Schmelz, 2024; Talagas et al, 2020a; Xu et al, 2022). Transfer of virus between keratinocytes and neurons has been demonstrated for neurotropic alphaherpesviruses (Smith, 2012; Wang et al, 2010). Given the observation that keratinocytes can become naturally infected with RABV, the potential for viral transfer to neurons represents a critical factor in assessing the risk associated with superficial RABV exposure. To address this, in the final part of our study, we developed an in vitro transwell model to investigate whether RABV-infected keratinocytes are capable of transmitting the virus to neuronal cells through direct cell−cell contact. Collectively, this study aimed to characterize RABV infection of keratinocytes in vitro, evaluate their antiviral response, and explore their potential role in facilitating viral entry into to the nervous system.

RESULTS

Human keratinocytes are permissive to RABV infection in vitro

Human epidermal keratinocytes of the cell line HaCaT and HPEKs were found to be susceptible to RABV strains dogRV, SHBRV, and SAD P5 (Figure 1a). Seventy-two hours after infection, up to 5 and 10% of HaCaT cells were infected with SHBRV or SAD P5, respectively, at a multiplicity of infection (MOI) of 1, as measured by intracellular expression of the RABV nucleoprotein (RABV-N) (Figure 1b). In contrast, <0.02% of cells were infected with dogRV at an MOI of 1. HPEKs showed higher susceptibility to all strains than HaCaT, with average infection rates of 8% (dogRV), 30% (SHBRV), and 20% (SAD P5) at an MOI of 1. Interestingly, 1 of the donors showed very low susceptibility to all 3 strains. We quantified the expression of the genes encoding for the potential RABV entry receptors nAChRa7, NCAM, p75NTR, mGluR2, and ITGB1 by qPCR. All tested receptors were expressed to similar levels by HaCaT and HPEKs (Supplementary Figure S1).

Whereas only single cells were infected with dogRV, SHBRV showed a focal pattern of infected cells, with increasing size at later time points after infection, suggesting cell-to-cell spread (Figure 1a and Supplementary Figure S2). The infection with SAD P5 was more widespread throughout the cell layer from early time points onward.

The infection with SHBRV and SAD P5 was productive, as demonstrated by the increase in infectious virus particles in culture supernatants (Figure 1c). The average increase in log(TCID50/ml) viral titers 120 hours after infection ranged from 1.2 (HaCaT infected with SAD P5 at MOI of 1) to 3.9 (HaCaT infected with SHBRV at MOI of 0.1). We did not find an increase in viral titers in the supernatants of HaCaT cells infected with dogRV and only a minor increase of 0.6 log(TCID50/ml) in the supernatants of HPEKs infected with dogRV 120 hours after infection. The neuroblastoma cell line SH-SY5Y, which was included as a positive control for infection, was confirmed to be highly susceptible to all 3 RABV strains (Supplementary Figure S3).

Keratinocytes upregulate immunorelevant surface markers after exposure to SHBRV and SAD P5 but not dogRV

To assess keratinocyte activation in response to virus exposure, we measured surface expression levels of ICAM-1, PD-L1, HLA-ABC, and HLA-DR (Figure 2a). These markers are typically found upregulated upon acute activation of keratinocytes and are relevant for immune cell recruitment and activation or, in the case of PD-L1, counter-regulating excessive immune activation (Black et al, 2007; Kroh et al, 2024; Okiyama and Katz, 2014). Stimulation with polyinosinic-polycytidylic acid, a synthetic analog of double-stranded RNA (Alexopoulou et al, 2001), was used as positive control. Neither cell type demonstrated upregulation of surface marker expression after exposure at MOI of 0.1. However, MOI of 1 exposure led to upregulation of PD-L1 in HaCaT cells but not in HPEKs for all 3 RABV strains. In

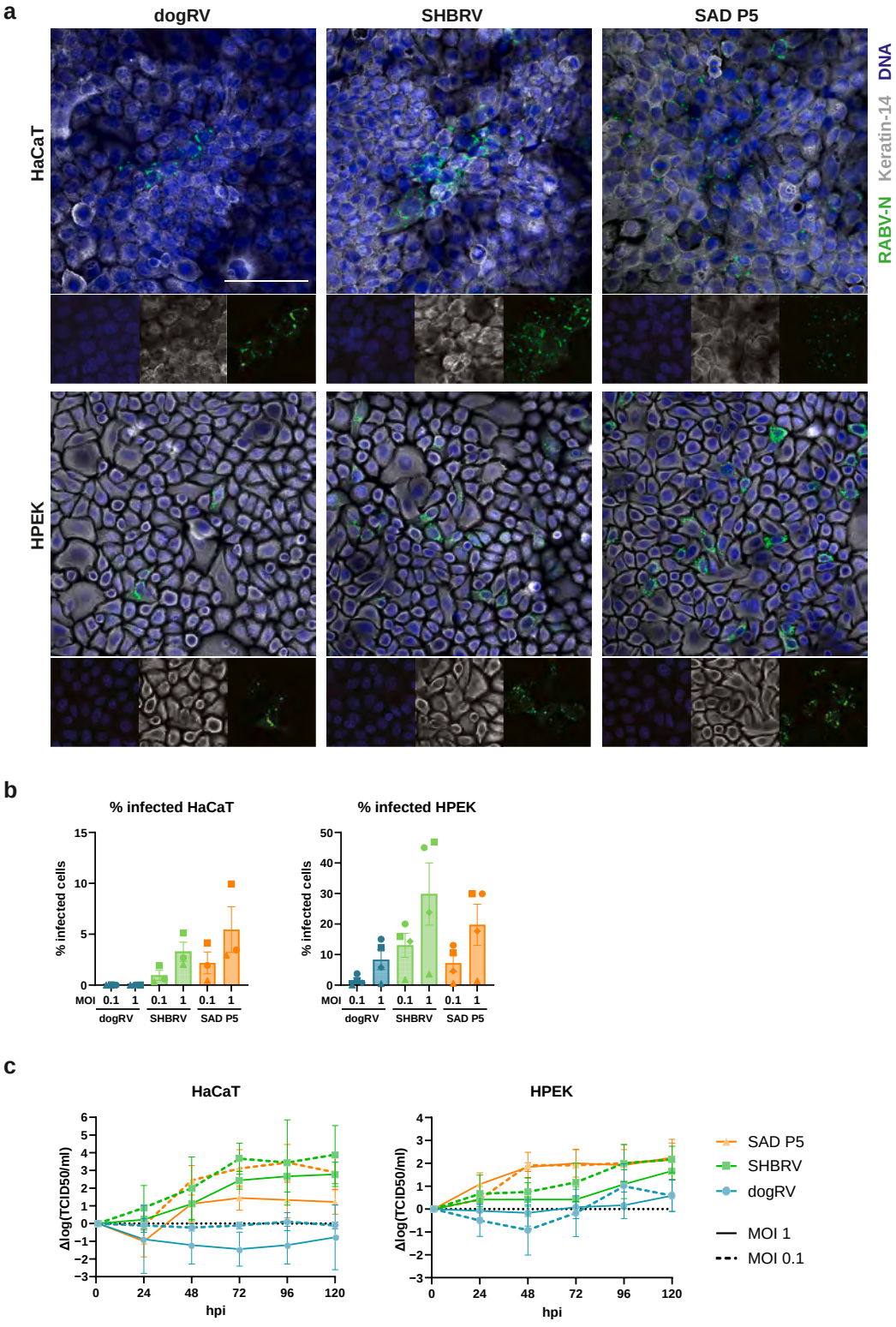

Figure 1. Susceptibility of keratinocytes to RABV infection in vitro. HaCaT and HPEKs were exposed to RABV strains dogRV, SHBRV, and SAD P5, at MOIs of 0.1 and 1. **(a)** Immunofluorescent staining for infection of keratinocytes at an MOI of 1 at 72 hpi. Bar = 100 μm. **(b)** Percentages of infected keratinocytes, determined by flow cytometry using intracellular anti−RABV-N staining, at 72 hpi. Bars show mean values ± SEM, and symbol shapes correspond to independent experiments (HaCaT) or individual donors (HPEKs). **(c)** Viral titers in culture supernatants. Values are shown as Δlog(TCID50/ml), representing the increase or decrease in viral titers compared with 1 hpi. Data are shown as mean ± SD. n = 3 independent experiments (HaCaT); n = 4 individual donors (HPEKs). dogRV, dog-related rabies virus; HPEK, human primary epidermal keratinocyte; hpi, hour after infection; MOI, multiplicity of infection; RABV, rabies virus; RABV-N, rabies virus nucleoprotein; SHBRV, silver-haired bat rabies virus.

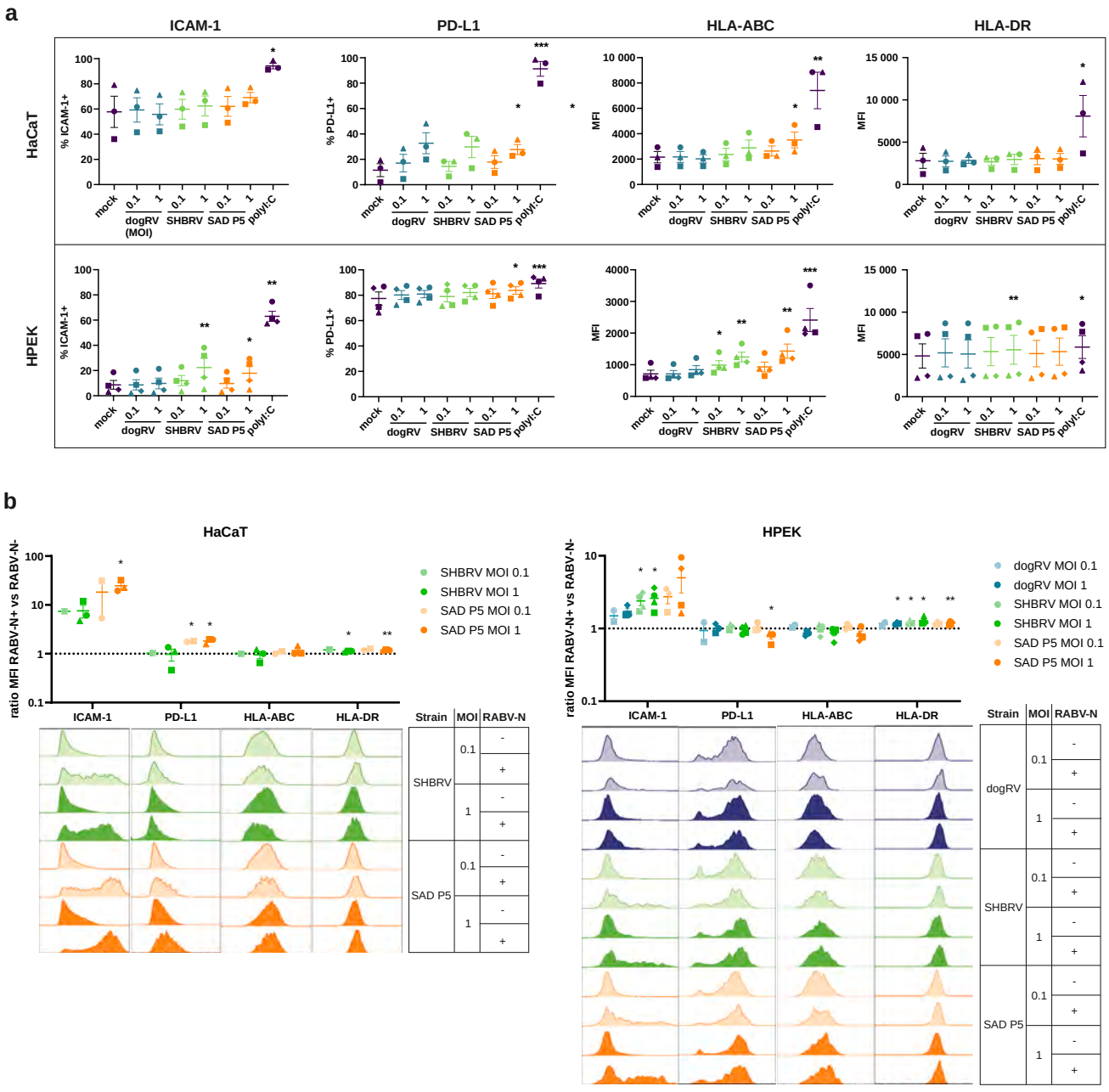

Figure 2. Surface activation marker expression of keratinocytes after RABV exposure. (**a**) Percentage of HaCaT or HPEK-positive cells for ICAM-1 or PDL-1 and MFI of HLA-ABC and HLA-DR, measured using flow cytometry at 72 hpi for the complete live cell population. Statistical significance was determined using Friedman test and Dunn's uncorrected multiple comparison test with the mock as control condition. (**b**) RABV-N+/RABV-N− population mean MFI ratios and representative histograms. Only samples with infection rates >1 % were included. One sample *t*-tests determined whether ratios of RABV-N+ versus RABV-N− cell populations differed significantly from 1. Lines represent mean values ± SEM, and symbol shapes represent independent experiments (HaCaT, n = 3) or donors (HPEK, n = 4). ***$P \leq .001$, **$P \leq .01$, and *$P < .05$. HPEK, human primary epidermal keratinocyte; hpi, hour after infection; MFI, median fluorescence intensity; MOI, multiplicity of infection; RABV, rabies virus; RABV-N, rabies virus nucleoprotein.

HPEKs, ICAM-1 and HLA-ABC were significantly upregulated after exposure to SHBRV and SAD P5 at an MOI of 1.

In addition, cells were gated into "infected" (RABV-N+) and "uninfected" (RABV-N−) populations (Supplementary Figure S4), and the surface marker expression was determined for each population individually. To assess whether the cell populations showed different activation, the ratio of the median fluorescence intensity levels of the infected versus the uninfected population was calculated for each marker (Figure 2b). Only samples where the infection percentage was >1% were included in the analysis. A strikingly higher expression of ICAM-1 in the infected population than in the uninfected population was observed for both cell types, with up to a 32-fold increase in HaCaTs and up to a 10-fold increase in HPEKs. PD-L1 expression was also significantly higher in SAD P5−infected than in uninfected HaCaT cell

populations but was decreased in SAD P5—infected HPEK populations (MOI of 1). HLA-DR showed an approximately 1.2-fold upregulation in infected versus uninfected cell populations, which was statistically significant for both HaCaT and HPEKs infected with SAD-P5 and SHBRV at an MOI of 1 and for HPEKs infected with SHBRV at an MOI of 0.1 and dogRV at an MOI of 1.

SAD P5 and SHBRV exposure leads to increased cytokine release by primary keratinocytes

To gain further insight into the antiviral response of RABV-exposed keratinocytes, we measured the concentration of 13 cytokines in culture supernatants (Figure 3 and Supplementary Figure S4) 72 hours after infection. The selection of the most significantly differentially released cytokines IFN-α2, IFN-λ1, IP-10, and IL-8 demonstrates that HaCaT cells display only a limited cytokine response to RABV exposure, with concentrations mostly comparable with those of the mock controls. Nevertheless, concentrations of IFN-α2 and IP-10 were significantly increased upon SAD P5 exposure and of IFN-λ1 upon SAD P5 and SHBRV exposure, at the high MOI of 1. For HPEKs, a clear increase in secreted concentrations was observed for IFN-α2, IFN-λ1, IP-10, IL-8, IL-6, and GM-CSF in response to SHBRV and SAD P5 at the MOI of 1, demonstrating a measurable antiviral response. To a lesser extent, this was observed for HPEKs exposed to SHBRV at the lower MOI of 0.1 as well. In addition, exposure of HPEKs to SHBRV at an MOI of 1 led to significantly increased release of IFN-β, IL-1β, and IL-10 (Supplementary Figure S5).

RABV passed from infected keratinocytes to neurons in a transwell coculture model

With previous experiments demonstrating the susceptibility of keratinocytes to RABV infection and indicating the induction of an antiviral response, the following experiments aimed to understand the potential for transmission from infected keratinocytes to neurons. To gain insight into the potential contact between infected keratinocytes and neurons in tissue, skin sections of mice experimentally infected with SHBRV intradermally through the footpad (Kroh et al, 2025a) were costained for RABV-N and the pan-neuronal marker PGP9.5 (Figure 4a). The tissue was sampled from the inoculation site, after the mice were killed at clinical endpoint. These stainings revealed that thin nerve fibers were present throughout the epidermis and sometimes colocalized with patches of infected keratinocytes.

On the basis of these observations, we developed a transwell coculture model using HaCaT cells on the apical side and the neuronal cell line SH-SY5Y on the basolateral side of a 3-μm porous membrane, simulating the contact of keratinocytes and neurons through direct cell—cell contact (Figure 4b). Virus was added to the apical compartment to infect the keratinocytes. The bat-derived RABV strain SHBRV was chosen for these experiments because it was considered the most relevant for addressing the question of superficial RABV transmission through the skin. HaCaT cells were selected for the model over HPEKs for the following reasons: lack of donor variability, medium compatibility with SH-SY5Y cells, and a focal infection pattern with SHBRV. H&E stainings of vertical cross-sections of the transwell insert revealed that the HaCaT cells grew in multiple layers, morphologically resembling the epidermis with rectangular cells on the basal side and flattened cells on the apical side (Figure 4c). Measurement of the transepithelial electrical resistance (TEER) and dextran leakage showed that HaCaT cells formed a tight barrier at the time of inoculation and that RABV infection did not impact barrier integrity (Figure 4d and Supplementary Figure S6). These data further show that the barrier is formed mainly by the HaCaT cells, with the presence of SH-SY5Y cells contributing only marginally to the TEER.

Levels of infectious virus particles were quantified in both compartments after 1 hour of infection and 48, 72, and 96 hours after infection (Figure 4e). With blank (cell-free) inserts, the virus passed through the pores freely and was detected in both compartments 1 hour after infection. Adding virus to the apical compartment in the absence of HaCaT cells led to high viral titers in both compartments starting 48 hours after infection, likely owing to high virus production by SH-SY5Y cells. For the cocultures, an increase in viral titers in the basolateral compartment was observed for 2 of 3 independent replicate experiments 48 hours after infection but to lower levels than detected for the inserts with only SH-SY5Y cells. One hour after infection, no virus was detected in the basolateral compartment, demonstrating that the HaCaT barrier was tight. For these 2 experiments, inserts with only HaCaT cells without SH-SY5Y cells were available. In this study, an increase in titers was detectable only after 72—96 hours after infection, demonstrating the low level of virus production into the basolateral compartment when only HaCaT cells are present.

Staining of vertical cross-sections of the transwell inserts (Figure 4f and Supplementary Figure S7) for RABV antigen showed virus presence mostly in superficial keratinocyte layers. However, viral antigen was also detected in the more basal keratinocyte layers and, occasionally, the underlying SH-SY5Y cells. In absence of HaCaT cells, the infection was widespread throughout the SH-SY5Y cells. This was visible using both an anti—RABV-N antibody for immunofluorescence and the more sensitive anti-RABV phosphoprotein antibody for immunohistochemistry.

DISCUSSION

RABV typically enters the host through disruptions of the skin or mucosal barriers, most commonly through dog bites (Fooks et al, 2017). Although neuromuscular junctions are considered the primary site of RABV entry into the CNS (Hemachudha et al, 2013), sensory neuron fibers innervating the punctured skin could pose another entry site (Begeman et al, 2018; Velandia-Romero et al, 2013). In our previous work, we identified the presence of RABV-infected keratinocytes at the site of inoculation of experimentally infected mice and at the probable infection site of naturally infected dogs (Kroh et al, 2025a). For this explorative follow-up study, we aimed to elucidate the implications of keratinocyte infection by addressing 2 primary questions: (1) How do keratinocytes respond to RABV exposure and (2) can RABV be transmitted from infected keratinocytes to neurons? Importantly, we also considered potential differences between RABV strains associated with different reservoir species.

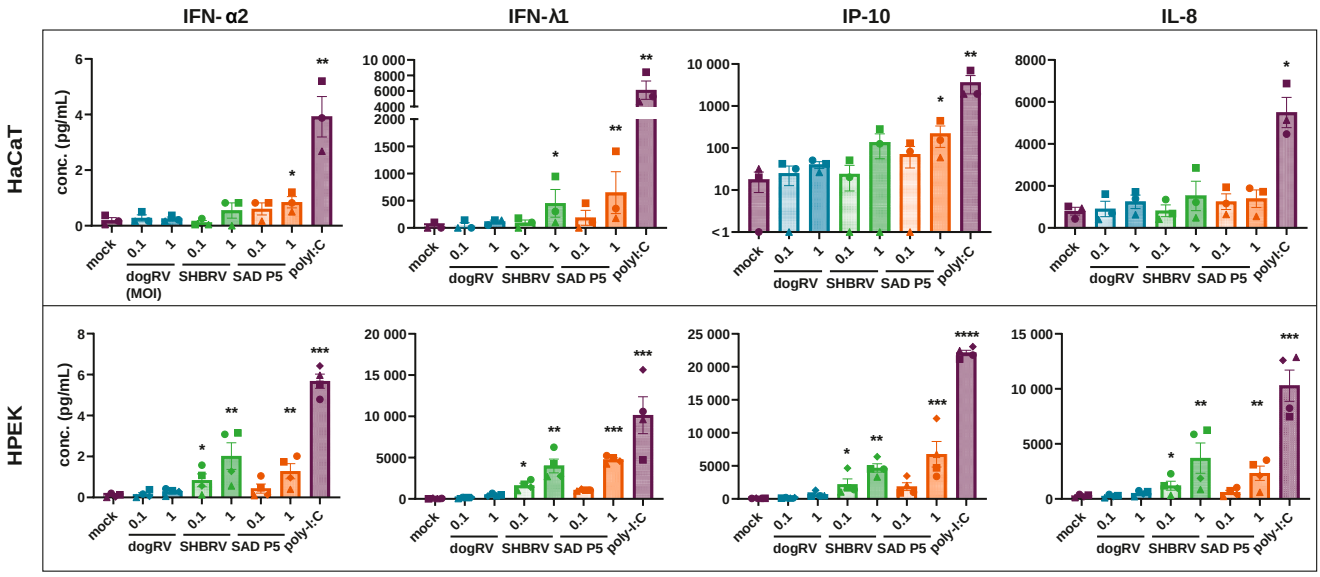

Figure 3. Concentration of selected cytokines in the supernatants of RABV-exposed keratinocytes. Cytokines were measured in supernatants taken at 72 hpi using a commercial multiplex bead-based assay. MOIs of 0.1 and 1 were used for infection as indicated. Supernatants of mock-inoculated cells and poly-I:C–stimulated cells (5 μg/mL) were taken along as negative and positive controls, respectively. Bars represent mean values ± SEM, and symbol shapes correspond to independent experiments (HaCaT, n = 3) or individual donors (HPEK, n = 4). Statistical significance was determined using Friedman test and Dunn's uncorrected multiple comparison test, with the mock as control condition. ****$P \leq .0001$, ***$P \leq .001$, **$P \leq .01$, and *$P < .05$. HPEK, human primary epidermal keratinocyte; hpi, hour after infection; MOI, multiplicity of infection; poly-I:C, polyinosinic-polycytidylic acid; RABV, rabies virus.

We observed marked differences in the susceptibility of keratinocytes to the different RABV strains that were used in this study. The much lower susceptibility of dogRV than SHBRV might reflect the origin of the strains—whereas canine-related strains are most likely transmitted through deep muscle-penetrating bites, bat-related strains could be more adapted to superficial inoculation (Hemachudha et al, 2013; Morimoto et al, 1996). The efficient infection by SAD P5 could result from its attenuation through repeated cell culture passaging (Höper et al, 2015; Sacramento et al, 1992). Multiple reasons have been proposed to explain differences in cellular tropism, including differences in G protein binding to host cell receptors, G protein expression, or sensitivity to the host cell immune response (Feige et al, 2022; Huang et al, 2017; Khalifa et al, 2021; Yang et al, 2015). Functional studies are needed to determine the factors involved in the differential tropism of the strains used in our study.

We observed a moderate but significant activation of keratinocytes in response to SHBRV and SAD P5 exposure, particularly at higher MOIs. This activation was evidenced by upregulation of immune-related surface markers and increased cytokine release, suggesting that keratinocytes are capable of mounting an antiviral response that may help limit RABV dissemination. RABV phosphoprotein, RABV-N, and RABV matrix proteins have been recognized for their IFN antagonistic functions (Ito et al, 2016). Whereas some studies have indicated greater immunosuppressive capacities of street RABV strains than attenuated strains (Masatani et al, 2016; Wang et al, 2005), other studies have found the opposite relationship (Niu et al, 2013). In our study, an activation response was measured for the pathogenic SHBRV strain and the apathogenic SAD P5 strain but not for the pathogenic dogRV strain, supporting that, indeed, an induction of the IFN response is highly strain specific and does not necessarily correlate with its pathogenicity. Further mechanistic studies are needed to study the activation of antiviral pathways in our keratinocyte models as well as the functionality of the IFN response. In our experiments, the extent of keratinocyte activation positively correlated with infection levels, a pattern similarly observed in dendritic cells and possibly associated with the production of viral leader RNA and RIG-I activation (Hornung et al, 2006; Kroh et al, 2025b; Yang et al, 2015). Notably, keratinocyte activation was not limited to infected cells, indicating a bystander effect likely mediated by cytokine signaling. This is supported by our finding that all tested surface markers, except ICAM-1, were only marginally differentially expressed between infected and uninfected cell populations. IFN-λ1, for instance, which was significantly upregulated upon RABV exposure, has indeed been shown to induce a proinflammatory response in keratinocytes (Goel et al, 2020).

Keratinocyte activation has been reported for viruses with the skin as primary replication site, such as dengue virus and alphaherpesviruses (Duangkhae et al, 2018; Milora et al, 2014; Shao et al, 2010). However, keratinocyte activation at the site of viral entry is likely influenced by additional factors besides direct virus exposure, such as tissue damage or components of animal saliva (Goldstein, 1992; Kishibe et al, 2015; Rodrigues Neves et al, 2019). Moreover, although activated keratinocytes may recruit immune cells, this alone may not be sufficient to initiate a robust adaptive immune response. RABV is reported to have a suppressive effect on immune cells (Embregts et al, 2021; Katz et al, 2017; Kroh et al, 2025b), which could impair downstream signaling and T-cell activation, even in the presence of keratinocyte-derived cues.

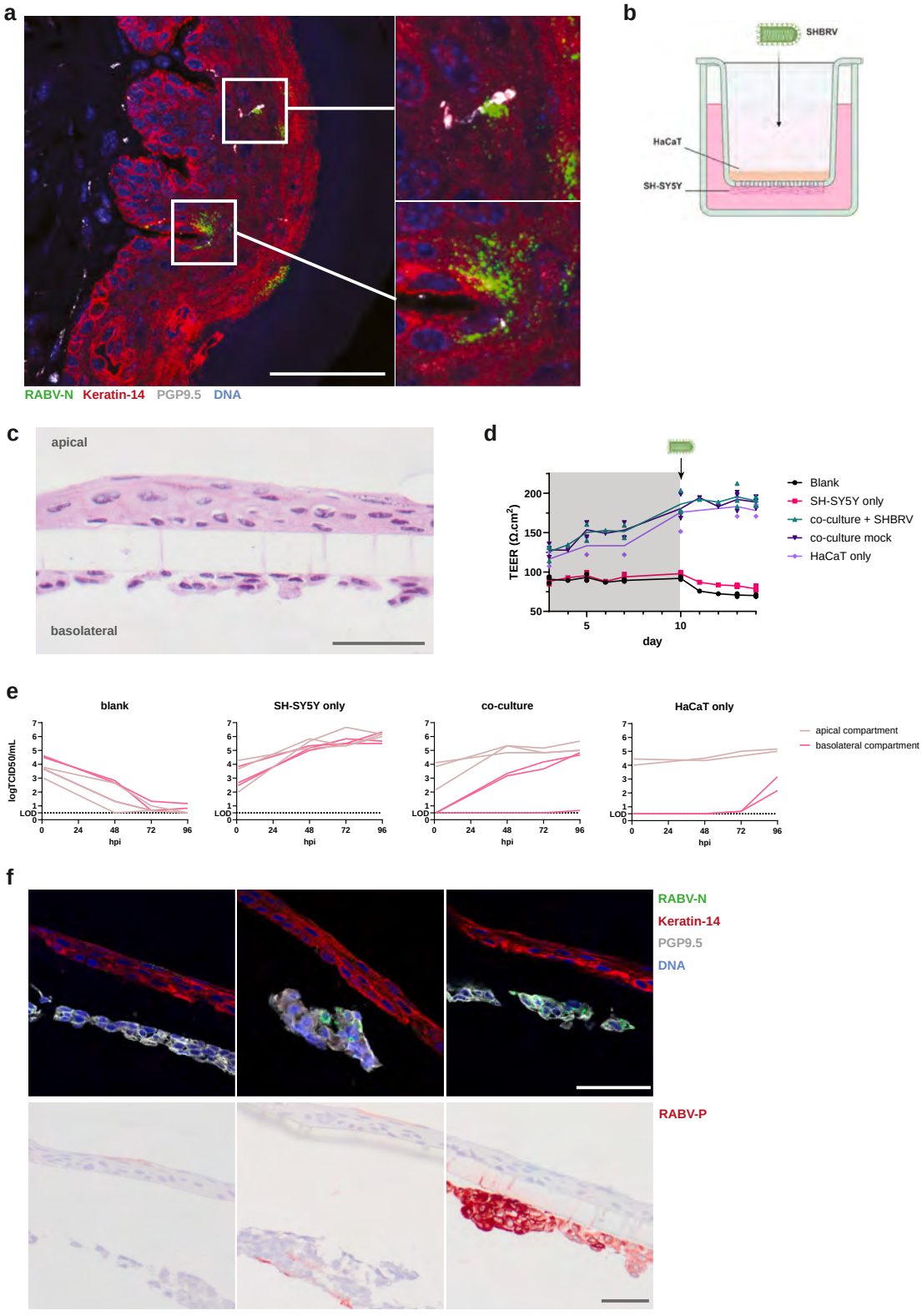

Figure 4. Transmission of RABV particles from infected keratinocytes to neurons in a transwell coculture model. (**a**) Localization of nerve endings (PGP9.5, white) and RABV (RABV-N, green) in the epidermis (keratin 14, red) of footpads of mice experimentally infected with SHBRV. (**b**) Schematic of the transwell model. (**c**) H&E staining of vertical cross-sections of the coculture. (**d**) Barrier integrity of the coculture system, before (gray) and after infection with SHBRV, measured using TEER. (**e**) Viral titers in the apical and basolateral transwell compartments at 48, 72, and 96 hpi, with no cells present (blank), HaCaT or SH-SY5Y cells alone, or both (coculture). (**f**) Immunofluorescence imaging of coculture cross-sections at 96 hpi, showing infection (RABV-N, green) of the upper HaCaT layer (keratin 14, red) and the SH-SY5Y layer (PGP9.5, white), and immunohistochemistry showing RABV-P antigen (red). Images show different replicates of the same condition. Bar = 50 μm. hpi, hour after infection; LOD, limit of detection; PGP9.5, protein gene product 9.5; RABV, rabies virus; RABV-N, rabies virus nucleoprotein; RABV-P, rabies virus phosphoprotein; SHBRV, silver-haired bat rabies virus; TEER, transepithelial electrical resistance.

We showed colocalization of intraepidermal nerve endings and infected keratinocytes in the footpad of experimentally infected mice, suggesting that viral transmission could be possible. To investigate this further, we used a proximal transwell coculture system in which HaCaT cells and the neuronal cell line SH-SY5Y were seeded on the apical and basolateral faces of a transwell membrane to model more direct cell−cell contact. The detection of infectious virus particles in the basolateral compartment, along with the presence of viral antigen in SH-SY5Y cells, supports the hypothesis that RABV could indeed pass from infected keratinocytes to neuronal cells. TEER measurements and the visualization of a continuous HaCaT barrier in cross-section images confirmed its integrity, indicating that viral passage occurred through transcellular transport. When only HaCaT cells were seeded, virus was detected in the basolateral compartment significantly later than in the coculture conditions. Minimal amounts of virus might be passed through the keratinocytes at early time points without detectable release into the supernatant but could be sufficient to infect the highly susceptible SH-SY5Y cells through direct contact. Although we did observe RABV antigen in basal keratinocyte layers in our model, it was predominantly confined to the superficial layers. This may help explain why minor exposures rarely result in rabies (Dato et al, 2016). In our previous study, application of virus to intact, brushed, or superficially scratched mouse ear skin did not result in infection (Kroh et al, 2025a). Multiple factors might play role, such as the thickness of the more terminally differentiated epidermal layers that might be less susceptible to viral infection. In addition, an intrinsic antiviral response of the keratinocytes could have limited further spread. Thus, we propose that successful RABV transmission through infected keratinocytes requires 2 factors: proximity to nerve endings and evasion of local immune defenses.

The precise mechanism of RABV transfer between keratinocytes and neurons in the skin remains to be elucidated. Herpesviruses are considered to transfer through shedding (Tsalenchuck et al, 2014), and ultrahigh-resolution imaging has shown that intraepidermal free nerve endings are engulfed by keratinocyte cytoplasmic tunnels (Talagas et al, 2020a), potentially facilitating viral transfer. RABV has been reported to replicate locally in muscle tissue prior to neuroinvasion (Murphy and Bauer, 1974; Yamaoka et al, 2013), a process that may similarly occur in the skin. The proposed presence of synaptic-like contacts between keratinocytes and intraepidermal nerve endings (Talagas et al, 2020b; Xu et al, 2022) could serve a role analogous to the neuromuscular junction in RABV pathogenesis. To our knowledge, our in vitro coculture model is the first to study RABV entry to the nervous system across a cell barrier. The proximity of the SH-SY5Y cell bodies to the HaCaT cells allows the study of virus transfer through cell−cell contact, whereas the use of cell lines makes this an easy-to-use and reproducible model. However, sensory neurons in the skin are in contact with keratinocytes through their axonal terminals rather than their cell bodies. Therefore, future models may simulate the intraepidermal nerve endings more accurately through the use of stem cell−derived sensory neurons and compartmented coculture systems as well as the use of primary keratinocytes.

In conclusion, this study provides insights into the role of keratinocytes in RABV pathogenesis. Using both cell line and primary keratinocyte in vitro models, we demonstrate their susceptibility and antiviral response to RABV infection. Importantly, we show that infected keratinocytes are capable of transmitting virus to neurons in vitro, indicating a potential role in superficial RABV transmission. These findings enhance our understanding of the viral−host interactions involved at the peripheral infection site and underscore the importance of prompt and appropriate postexposure prophylaxis, even after minor exposures. Future in-depth studies should be performed to provide mechanistic insight into the differential strain tropism, the interactions of infected keratinocytes with immune cells, and the mechanisms of neuroinvasion from superficial skin contact.

MATERIALS AND METHODS

Cells

Human keratinocyte HaCaT cells (Boukamp et al, 1988) were obtained from CLS Cell Lines Service GmbH. Cells were cultured in DMEM (Capricorn Scientific) supplemented with 10% (v/v) fetal calf serum (Sigma-Aldrich), 1x penicillin/streptomycin (Capricorn Scientific), and 2 mM L-glutamine (Capricorn Scientific) at 37 °C and 5% carbon dioxide.

HPEKs were isolated as described previously (Helgers et al, 2024). Briefly, 0.3 mm skin grafts, obtained from donors undergoing corrective surgery performed at Boerhaave Medical Center (Amsterdam, The Netherlands), were obtained using a dermatome (Zimmer Biomet). After overnight incubation with Dispase II (1 U/ml, Roche Diagnostics) at 4 °C, the epidermis was separated from the dermis. The epidermis was cut and incubated with 0.05% Trypsin (Beckton Dickinson) and DNase I (20 units/ml, Roche Applied Science) for 30 minutes at 37 °C. Single-cell suspensions were obtained by mechanical disruption of the epidermis. HPEKs were cultured in DermaLife K cell culture medium (Lifeline Cell Technology), supplemented with the provided DermaLife K LifeFactors Kit and antimicrobial supplement and 1x penicillin/streptomycin at 37 °C with 5% carbon dioxide. Medium was changed every 3−4 days, and cells were passaged at 80% confluency by 15-minute incubation with 0.05% Trypsin-EDTA at 37 °C. Cells were used for experiments at passages 2 and 3 (2 donors each) in 1 single experiment. Keratinocyte purity was confirmed to be >95% by immunofluorescence using an anti−keratin 14 antibody or by flow cytometry using an anti−pan-cytokeratin antibody for the respective experiments; methods are described below.

Cells of the neuroblastoma cell line SH-SY5Y (Sigma-Aldrich) were cultured in Advanced DMEM/F12 (Gibco) supplemented with 10% (v/v) fetal calf serum, 1x penicillin/streptomycin, 2 mM L-glutamine, 1x nonessential amino acids (Capricorn Scientific), and 0.8 mg/ml sodium bicarbonate (Gibco) at 37 °C and 5% carbon dioxide.

Viruses

SHBRV is commonly used as pathogenic street RABV strain in experimental infections and immunological investigations (Embregts et al, 2023; Kroh et al, 2025b; Marosi et al, 2019). DogRV was isolated from a patient who died from dog-associated rabies (Oude Munnink et al, 2020). The attenuated vaccine−based strain SAD P5/88 Potsdam (SAD P5) was sourced from Institute Pasteur (Paris, France) through EVAg (European Virus Archive Global) repository

(isolate 9509TCH, ref-SKU 014V-01931). Viruses were grown on SH-SY5Y cells and used for experiments at passage numbers 2–5.

For experimental infection, HaCaT or HPEKs were seeded in suitable plates at a density of approximately 1×10^5 cells per cm^2 1 day prior to infection. Cells were incubated with virus in serum-free medium for 1 hour at 37 °C, after which the inoculum was aspirated and replaced with fresh complete medium. Mock controls were incubated with serum-free medium without virus. Incubation with 5 μg/mL high-molecular-weight polyinosinic-polycytidylic acid (Invitrogen) was used as positive control for cell activation.

$TCID_{50}$ endpoint dilution assay

Infectious virus particles in culture supernatants were quantified using the $TCID_{50}$ (median tissue culture infective dose) endpoint dilution method of Reed and Munch (Reed and Muench, 1938). Briefly, samples were added to SH-SY5Y cells at 10-fold serial dilutions in serum-free medium for 1 hour at 37 °C, after which the medium was replaced with complete medium. The cells were fixed 72 hours after infection using 80% acetone and stained using FITC-conjugated anti–RABV-N antibody (Fujirebio) and nuclei counterstaining using Hoechst (Invitrogen). Wells were scored positive when at least 1 cell was clearly positively stained for RABV-N. One hour after infection timepoint samples, supernatant was taken after the 1-hour incubation period with the virus, after removal of the inoculum and replacement with fresh medium.

Flow cytometry

Seventy-two hours after infection, keratinocyte single-cell suspensions were obtained by trypsinization as described earlier. Cells were washed with PBS and incubated with Zombie Aqua fixable viability stain (BioLegend) for 30 minutes at room temperature. After washing with FACS buffer (PBS, 2% fetal calf serum, 2 mM EDTA), cells were incubated with antibodies anti–CD54-PE/Cyanine7 (clone HA58); anti–PD-L1-Brilliant Violet 785 (clone 29E.2A3); anti–HLA-DR-APC/Cyanine7 (clone L243); and anti–HLA-A,B,C-Brilliant Violet 605 (clone W6/32, all from BioLegend) for 30 minutes at 4 °C. Cells were fixed and permeabilized using the Cytofix/Cytoperm kit (BD Biosciences) according to manufacturer's instructions and stained intracellularly with anti–RABV-N-FITC (Fujirebio) for 30 minutes at 4 °C. HPEKs were additionally stained with anti–pan-cytokeratin-PE (C-11, Thermo Fisher Scientific). Cells were analyzed using the FACSLyric flow cytometer (BD Biosciences) and FlowJo V10 software (FlowJo LLC).

Multiplex cytokine quantification

Concentrations of cytokines GM-CSF, IFN-α2, IFN-β, IFN-λ1, IFN-λ2/3, IFN-γ, IL-1β, IL-6, IL-8, IL-10, IL-12p70, IP-10, and TNF-α in cell culture supernatants were quantified using the LEGENDplex Human Anti-Virus Response Panel 13-plex bead-based immunoassay kit (BioLegend), according to manufacturer's instructions. Subsequently, beads were fixed for 25 minutes using the Cytofix/Cytoperm solution (BD Biosciences). Fluorescence signals were measured using a FACSLyric flow cytometer (BD Biosciences) and analyzed using the LEGENDplex Data Analysis Software Suite (BioLegend). Values outside limit of detection were extrapolated on the basis of standard curves.

Transwell coculture model

For the transwell coculture model, HaCaT and SH-SY5Y cells were seeded on either sides of ThinCert 12-well inserts with a 3-μm pore transparent membrane (Greiner) using a protocol adapted from Marshall et al (2024). SH-SY5Y cells were seeded at a density of 50,000 cells on the basolateral side of the membrane. After allowing cells to attach for 4–6 hours, HaCaT cells were added to the apical side at a density of 125,000 cells. As controls, inserts were left blank (no cells added), and only SH-SY5Y or only HaCaT cells were seeded. A total volume of 1200 μl of SH-SY5Y medium was added to the bottom compartment, and 800 μl of HaCaT medium was added to the top compartment. Medium was changed every 3–4 days. The TEER was measured every 2–4 days to monitor barrier integrity as described below. Cells were infected from the apical side on day 10 after seeding with an MOI of 1. Medium was removed from both compartments, and fresh SH-SY5Y medium was added to the bottom compartment. SHBRV was added in 100 μl of serum-free medium to the top compartment. After 1 hour, medium was replaced with 800 μl of fresh HaCaT medium. Supernatant from both compartments was taken after medium replacement for virus quantification for the 1-hour time point. Every 24 hours, 100 μl of supernatant was removed for virus quantification and replaced with 100 μl of fresh medium. TEER was measured before infection and 72 and 96 hours after infection. Ninety-six hours after infection, transwell inserts were fixed using 80% acetone for 1 hour. Inserts were washed twice with PBS and stored in PBS until further use. Transwells were used in duplicates per experiment, and 3 independent experiments were performed.

TEER assay

The TEER of transwell cultures was measured using an EVOM2 Epithelial Voltohmmeter (World Precision Instruments) as described previously (Marshall et al, 2024). Briefly, STX2 TEER chopstick electrodes (World Precision Instruments) were disinfected with 70% ethanol for 5 minutes and afterward equilibrated in a series of deionized water, PBS, and culture medium. TEER was measured on 3 sides of the transwell inserts, and on each side, the lowest measured TEER was used to calculate average values. The values were normalized to the surface area for analysis.

Dextran assay

A total of 20 or 70 kDa fluorescent FITC dextran (Sigma-Aldrich) were added to the apical compartment of the transwell coculture to a final concentration of 100 μg/ml and incubated for 24 hours. Fluorescence in both compartments was measured using a Tecan Infinite F200 Pro. Dextran concentrations were calculated on the basis of a standard curve.

Murine skin tissue samples

Skin tissues were obtained from the inoculation sites (footpads) of mice that were intradermally infected with SHBRV. Mice were killed at clinical endpoint (showing neurological signs, starting on day 6 after inoculation) or at day 15 after inoculation. Samples were selected on the basis of previous detection of RABV in keratinocytes (Kroh et al, 2025a). Footpads were fixed and processed as described previously (Kroh et al, 2025a).

Immunohistochemistry staining

For imaging of transwell cocultures, membranes were cut out from the inserts and cut in 2 parts. Membranes were fixated in agarose and embedded in paraffin. Cross-sections were stained as described previously (Kroh et al, 2025a). Sections were incubated with anti–RABV phosphoprotein primary antibody (kindly provided by S. Finke [Orbanz and Finke, 2010]) or isotype control and horseradish peroxidase–conjugated secondary antibody. Revelation was done with 3-amino-9-ethylcarbazole. Slides were imaged using an

Table 1. Primer Sequences for RT-qPCR Detection of Target Gene Expression

Target Gene	Forward Primer (5′→3′)	Reverse Primer (5′→3′)
p75NTR (NGFR)	CCTCATCCCTGTCTATTGCTCC	GTTGGCTCCTTGCTTGTTCTGC
CD56 (NCAM1)	CATCACCTGGAGGACTTCTACC	CAGTGTACTGGATGCTCTTCAGG
CHRNA7 (α-subunit)	TGGTGACAGTGATCGTGCTGCA	GCCTCTTCATTCGCAGGAACCA
GRM2 (mGluR2)	CGGTTCCTACAGTGATGTCTCC	TGGCTTGGAAGAAGTCAGGAGG
ITGB1	GGATTCTCCAGAAGGTGGTTTCG	TGCCACCAAGTTTCCCATCTCC
TBP	GGGGAGCTGTGATGTGAAGT	CCAGGAAATAATTCTGGCTCA

Olympus BX51 light microscope and cellSens imaging software (Olympus).

Immunofluorescence staining

For immunofluorescence imaging of HaCaT and HPEK infection, cells were seeded and infected on 13-mm round glass coverslips (VWR). Acetone-fixed coverslips were stained with anti−keratin 14 (Poly19053, BioLegend) and anti−RABV-N-FITC (Fujirebio) primary antibodies for 1 hour at 37 °C. After washing, coverslips were incubated with anti-rabbit IgG-AF555 (Thermo Fisher Scientific) secondary antibody and Hoechst (Invitrogen) nuclei counterstain for 45 minutes at 37 °C. Coverslips were mounted on glass slides using Prolong Gold Antifade reagent (Thermo Fisher Scientific).

Transwell inserts were processed as described in the previous section. The following primary and secondary antibodies were used: anti−keratin 14 (Poly9060, BioLegend), anti−protein gene product 9.5 (rabbit polyclonal, Enzo Life Sciences), anti−RABV-N (5DF12 [Grassi et al, 1989]), anti-chicken IgY-AF555, anti-rabbit IgG-AF647, and anti-mouse IgG-AF488 (all from Invitrogen). Prior to primary antibody incubation, slides were incubated with TrueBlack Lipofuscin Autofluorescence Quencher (Biotium), diluted 1:1000, for 30 seconds and blocked with 5% normal goat serum (Dako)/5% normal donkey serum (Sigma-Aldrich) for 30 minutes. Nuclei were counterstained with Hoechst (Invitrogen). Slides were mounted using ProLong Gold Antifade reagent (Thermo Fisher Scientific).

Specimens were imaged using an LSM700 or LSM900 confocal laser-scanning microscope (Zeiss). Images were processed using ZEN 3.4 Software (Zeiss).

RT-qPCRs

Gene expression levels of RABV entry receptors *CHRNA7*, *NCAM1*, *NGFR*, *GRM2*, and *ITGB1* were measured by RT-qPCR. RNA was isolated from cell lysates using Agencourt AMPure XP beads (Beckman Coulter), according to the manufacturer's instructions. RNA was reverse transcribed into cDNA using the SuperScript IV Reverse Transcriptase kit (Thermo Fisher Scientific). Target amplification and detection were performed in the presence of SYBR Green (Thermo Fisher Scientific) with an ABI 7500 real-time PCR system. Primer sequences can be found in Table 1. Normalized threshold (denoted as Nt) values were calculated by normalizing to the expression of the household gene *TBP* (Nt = 2Ct[TBP]−Ct[target]).

Statistical analysis

Data visualization and statistical analysis were performed using the GraphPad Prism software (version 10.1.2). Mean values of the experimental conditions versus mock were compared using the Friedman test and uncorrected Dunn's multiple comparison test. One sample *t*-tests were performed to determine whether mean surface marker expression ratios of RABV-N+ versus RABV-N− cell populations differed statistically significantly from 1. *P*-values <0.05 were considered statistically significant.

ETHICS STATEMENT

Human skin tissue was obtained after written, informed consent in accordance with the Amsterdam University Medical Centres institutional guidelines with approval of the Medical Ethics Review Committee of the Amsterdam University Medical Centres, location Academic Medical Centre (Amsterdam, The Netherlands; reference number: W15_089 # 15.0103). All samples were handled anonymously. Murine skin samples were obtained from experiments that were performed under a project license (2019-0060) approved by the competent Dutch authority and in compliance with Dutch regulation for the protection of animals used for scientific purposes (implementing EU directive 2010/63) and other relevant regulations. The specific study protocol (18-7204-01) was approved by the institutional Animal Welfare Body.

DATA AVAILABILITY STATEMENT

The authors affirm that all data necessary for confirming the conclusions of the article are present within the article, figures, and tables. Raw data files are available from the corresponding author upon reasonable request.

ORCIDs

Keshia Kroh: http://orcid.org/0000-0002-9166-0711
Eleanor M. Marshall: http://orcid.org/0000-0002-1434-6438
Redwan Rahmat: http://orcid.org/0000-0003-2900-135X
Debby Schipper: http://orcid.org/0000-0001-6449-4765
Leanne C. Helgers: http://orcid.org/0000-0003-1200-2225
Teunis B. H. Geijtenbeek: http://orcid.org/0000-0002-5710-2839
Corine H. GeurtsvanKessel: http://orcid.org/0000-0002-7678-314X
Carmen W. E. Embregts: http://orcid.org/0000-0003-4710-9225

CONFLICT OF INTEREST

The authors state no conflict of interest.

ACKNOWLEDGMENTS

We thank the virus culture group at the unit of clinical virology (Viroscience Department, Erasmus MC) for technical support with performing the endpoint dilution assays. We thank S. Finke (Friedrich-Loeffler-Institut, Insel Riems, Germany) for providing the rabies virus phosphoprotein antibody. T. Kuiken and L. Begeman are acknowledged for scientific discussion. We thank Sharomy van den Rijen for her assistance in setting up the immunofluorescence staining of nerve endings in mouse tissues. The graphical abstract and Figure 4b were created in BioRender. 3, V. (2025) (https://BioRender.com/lz9qgrt and https://BioRender.com/maf5fr3). This work was funded through a VENI grant (to CWEE) from the Dutch Research Council (NWO-VENI 09150162010181).

Disclaimer

The funders did not play any role in the study design, data collection and analysis, decision to publish, or preparation of the manuscript.

AUTHOR CONTRIBUTIONS

Conceptualization: KK, CHG, CWEE; Formal Analysis: KK; Funding Acquisition: CHG, CWEE; Investigation: KK, ADB, RR, DS; Methodology: KK, EMM; Resources: LCH, TBHG; Supervision: CHG, CWEE; Visualization: KK; Writing − Original Draft Preparation: KK; Writing − Review and Editing: KK, ADB, EMM, RR, DS, LCH, TBHG, CWEE, CHG

DECLARATION OF GENERATIVE ARTIFICIAL INTELLIGENCE (AI) OR LARGE LANGUAGE MODELS (LLMs)

During the preparation of this work, the authors used Microsoft Copilot to improve clarity and readability of the manuscript, using the following prompt: "Provide feedback on the clarity and flow of this paragraph." After using this tool, the authors reviewed and edited the content as needed and take full responsibility for the content of the publication.

SUPPLEMENTARY MATERIAL

Supplementary material is linked to the online version of the paper at www.jidonline.org, and at 10.1016/j.jid.2026.01.036.

REFERENCES

Alexopoulou L, Holt AC, Medzhitov R, Flavell RA. Recognition of double-stranded RNA and activation of NF-kappaB by toll-like receptor 3. Nature 2001;413:732–8.

Begeman L, GeurtsvanKessel C, Finke S, Freuling CM, Koopmans M, Müller T, et al. Comparative pathogenesis of rabies in bats and carnivores, and implications for spillover to humans. Lancet Infect Dis 2018;18:e147–59.

Bharti OK, Chand R, Chauhan A, Rao R, Sharma H, Phull A. "Scratches/Abrasions without Bleeding" cause rabies: a 7 years rabies death review from medical college Shimla, Himachal Pradesh, India. Indian J Community Med 2017;42:248–9.

Black AP, Ardern-Jones MR, Kasprowicz V, Bowness P, Jones L, Bailey AS, et al. Human keratinocyte induction of rapid effector function in antigen-specific memory CD4+ and CD8+ T cells. Eur J Immunol 2007;37:1485–93.

Boukamp P, Petrussevska RT, Breitkreutz D, Hornung J, Markham A, Fusenig NE. Normal keratinization in a spontaneously immortalized aneuploid human keratinocyte cell line. J Cell Biol 1988;106:761–71.

Dato VM, Campagnolo ER, Long J, Rupprecht CE. A systematic review of human bat rabies virus variant cases: evaluating unprotected physical contact with claws and teeth in support of accurate risk assessments. PLoS One 2016;11:e0159443.

Duangkhae P, Erdos G, Ryman KD, Watkins SC, Falo LD Jr, Marques ETA Jr, et al. Interplay between keratinocytes and myeloid cells drives dengue virus spread in human skin. J Invest Dermatol 2018;138:618–26.

Embregts CWE, Begeman L, Voesenek CJ, Martina BEE, Koopmans MPG, Kuiken T, et al. Street RABV induces the cholinergic anti-inflammatory pathway in human monocyte-derived macrophages by binding to nAChr α7. Front Immunol 2021;12:622516.

Embregts CWE, Wentzel AS, den Dekker AT, van IJcken WFJ, Stadhouders R, GeurtsvanKessel CH. Rabies virus uniquely reprograms the transcriptome of human monocyte-derived macrophages. Front Cell Infect Microbiol 2023;13:1013842.

Feige L, Kozaki T, Dias de Melo G, Guillemot V, Larrous F, Ginhoux F, et al. Susceptibilities of CNS cells towards rabies virus infection is linked to cellular innate immune responses. Viruses 2022;15:88.

Fooks AR, Cliquet F, Finke S, Freuling C, Hemachudha T, Mani RS, et al. Rabies. Nat Rev Dis Primers 2017;3:17091.

Goel RR, Wang X, O'Neil LJ, Nakabo S, Hasneen K, Gupta S, et al. Interferon lambda promotes immune dysregulation and tissue inflammation in TLR7-induced lupus. Proc Natl Acad Sci USA 2020;117:5409–19.

Goldstein EJ. Bite wounds and infection. Clin Infect Dis 1992;14:633–8.

Grassi M, Wandeler AI, Peterhans E. Enzyme-linked immunosorbent assay for determination of antibodies to the envelope glycoprotein of rabies virus. J Clin Microbiol 1989;27:899–902.

Guo C, Li Y, Huai Y, Rao CY, Lai S, Mu D, et al. Exposure history, post-exposure prophylaxis use, and clinical characteristics of human rabies cases in China, 2006-2012. Sci Rep 2018;8:17188.

Hampson K, Coudeville L, Lembo T, Sambo M, Kieffer A, Attlan M, et al. Estimating the global burden of endemic canine rabies. PLoS Negl Trop Dis 2015;9:e0003709.

Helgers LC, Keijzer NCH, van Hamme JL, Sprokholt JK, Geijtenbeek TBH. Dengue virus infects human skin Langerhans cells through langerin for dissemination to dendritic cells. J Invest Dermatol 2024;144:1099–111.e3.

Hemachudha T, Ugolini G, Wacharapluesadee S, Sungkarat W, Shuangshoti S, Laothamatas J. Human rabies: neuropathogenesis, diagnosis, and management. Lancet Neurol 2013;12:498–513.

Höper D, Freuling CM, Müller T, Hanke D, von Messling V, Duchow K, et al. High definition viral vaccine strain identity and stability testing using full-genome population data–the next generation of vaccine quality control. Vaccine 2015;33:5829–37.

Hornung V, Ellegast J, Kim S, Brzózka K, Jung A, Kato H, et al. 5′-triphosphate RNA is the ligand for RIG-I. Science 2006;314:994–7.

Huang J, Zhang Y, Huang Y, Gnanadurai CW, Zhou M, Zhao L, et al. The ectodomain of rabies virus glycoprotein determines dendritic cell activation. Antiviral Res 2017;141:1–6.

Ito N, Moseley GW, Sugiyama M. The importance of immune evasion in the pathogenesis of rabies virus. J Vet Med Sci 2016;78:1089–98.

Jiang Y, Tsoi LC, Billi AC, Ward NL, Harms PW, Zeng C, et al. Cytokinocytes: the diverse contribution of keratinocytes to immune responses in skin. JCI Insight 2020;5:e142067.

Katz ISS, Guedes F, Fernandes ER, Dos Ramos Silva S. Immunological aspects of rabies: a literature review. Arch Virol 2017;162:3251–68.

Khalifa ME, Unterholzner L, Munir M. Structural and evolutionary insights into the binding of host receptors by the rabies virus glycoprotein. Front Cell Infect Microbiol 2021;11:736114.

Kishibe M, Griffin TM, Radek KA. Keratinocyte nicotinic acetylcholine receptor activation modulates early TLR2-mediated wound healing responses. Int Immunopharmacol 2015;29:63–70.

Kroh K, Barton J, Fehling H, Lotter H, Volkmer B, Greinert R, et al. Antimicrobial activity of NK cells to Trypanosoma cruzi infected human primary keratinocytes. PLoS Negl Trop Dis 2024;18:e0012255.

Kroh K, Rahmat R, Begeman L, van Greuningen LW, Schipper D, Ravensberg MF, et al. Exploring the role of infected keratinocytes during rabies virus infection. Npj Viruses 2025a;3:53.

Kroh K, Te Marvelde MR, van Greuningen LW, Laksono BM, Koopmans MPG, Kuiken T, et al. A comparative analysis of the dendritic cell response upon exposure to different rabies virus strains. PLoS Negl Trop Dis 2025b;19:e0012994.

Marosi A, Dufkova L, Forró B, Felde O, Erdélyi K, Širmarová J, et al. Combination therapy of rabies-infected mice with inhibitors of pro-inflammatory host response, antiviral compounds and human rabies immunoglobulin. Vaccine 2019;37:4724–35.

Marshall EM, Koopmans M, Rockx B. Usutu virus and West Nile virus use a transcellular route of neuroinvasion across an in vitro model of the human blood-brain barrier. Npj Viruses 2024;2:32.

Masatani T, Ozawa M, Yamada K, Ito N, Horie M, Matsuu A, et al. Contribution of the interaction between the rabies virus P protein and I-kappa B kinase ϵ to the inhibition of type I IFN induction signalling. J Gen Virol 2016;97:316–26.

Milora KA, Miller SL, Sanmiguel JC, Jensen LE. Interleukin-1α released from HSV-1-infected keratinocytes acts as a functional alarmin in the skin. Nat Commun 2014;5:5230.

Morimoto K, Patel M, Corisdeo S, Hooper DC, Fu ZF, Rupprecht CE, et al. Characterization of a unique variant of bat rabies virus responsible for newly emerging human cases in North America. Proc Natl Acad Sci USA 1996;93:5653–8.

Murphy FA, Bauer SP. Early street rabies virus infection in striated muscle and later progression to the central nervous system. Intervirology 1974;3:256–68.

Murphy FA, Harrison AK, Winn WC, Bauer SP. Comparative pathogenesis of rabies and rabies-like viruses: infection of the central nervous system and centrifugal spread of virus to peripheral tissues. Lab Invest 1973;29:1–16.

Niu X, Tang L, Tseggai T, Guo Y, Fu ZF. Wild-type rabies virus phosphoprotein is associated with viral sensitivity to type I interferon treatment. Arch Virol 2013;158:2297–305.

Okiyama N, Katz SI. Programmed cell death 1 (PD-1) regulates the effector function of CD8 T cells via PD-L1 expressed on target keratinocytes. J Autoimmun 2014;53:1–9.

Orbanz J, Finke S. Generation of recombinant European bat lyssavirus type 1 and inter-genotypic compatibility of lyssavirus genotype 1 and 5 anti-genome promoters. Arch Virol 2010;155:1631–41.

Oude Munnink BB, Farag EABA, GeurtsvanKessel C, Schapendonk C, van der Linden A, Kohl R, et al. First molecular analysis of rabies virus in Qatar and

clinical cases imported into Qatar, a case report. Int J Infect Dis 2020;96:323–6.

Pieracci EG, Pearson CM, Wallace RM, Blanton JD, Whitehouse ER, Ma X, et al. Vital signs: trends in human rabies deaths and exposures - United States, 1938-2018. MMWR Morb Mortal Wkly Rep 2019;68:524–8.

Reed LJ, Muench H. A simple method of estimating fifty per cent endpoints. Am J Epidemiol 1938;27:493–7.

Rodrigues Neves C, Buskermolen J, Roffel S, Waaijman T, Thon M, Veerman E, et al. Human saliva stimulates skin and oral wound healing in vitro. J Tissue Eng Regen Med 2019;13:1079–92.

Sacramento D, Badrane H, Bourhy H, Tordo N. Molecular epidemiology of rabies virus in France: comparison with vaccine strains. J Gen Virol 1992;73:1149–58.

Shao Y, Zhang W, Dong X, Liu W, Zhang CH, Zhang J, et al. Keratinocytes play a role in the immunity to herpes simplex virus type 2 infection. Acta Virol 2010;54:261–7.

Simani S, Fayaz A, Rahimi P, Eslami N, Howeizi N, Biglari P. Six fatal cases of classical rabies virus without biting incidents, Iran 1990-2010. J Clin Virol 2012;54:251–4.

Smith G. Herpesvirus transport to the nervous system and back again. Annu Rev Microbiol 2012;66:153–76.

Ständer S, Schmelz M. Skin innervation. J Invest Dermatol 2024;144:1716–23.

Talagas M, Lebonvallet N, Leschiera R, Elies P, Marcorelles P, Misery L. Intraepidermal nerve endings progress within keratinocyte cytoplasmic tunnels in normal human skin. Exp Dermatol 2020a;29:387–92.

Talagas M, Lebonvallet N, Leschiera R, Sinquin G, Elies P, Haftek M, et al. Keratinocytes communicate with sensory neurons via synaptic-like contacts. Ann Neurol 2020b;88:1205–19.

Tsalenchuck Y, Tzur T, Steiner I, et al. Different modes of herpes simplex virus type 1 spread in brain and skin tissues. J Neurovirol 2014;20:18–27.

Velandia-Romero ML, Castellanos JE, Martínez-Gutiérrez M. In vivo differential susceptibility of sensory neurons to rabies virus infection. J Neurovirol 2013;19:367–75.

Wang F, Zumbrun EE, Huang J, Si H, Makaroun L, Friedman HM. Herpes simplex virus type 2 glycoprotein E is required for efficient virus spread from epithelial cells to neurons and for targeting viral proteins from the neuron cell body into axons. Virology 2010;405:269–79.

Wang JN, Li M. The immune function of keratinocytes in anti-pathogen infection in the skin. Int J Dermatol Venereol 2020;3:231–8.

Wang ZW, Sarmento L, Wang Y, Li XQ, Dhingra V, Tseggai T, et al. Attenuated rabies virus activates, while pathogenic rabies virus evades, the host innate immune responses in the central nervous system. J Virol 2005;79:12554–65.

WHO. Rabies vaccines: WHO position paper, April 2018–Recommendations. Vaccine 2018;36:5500–3.

Xu X, Yu C, Xu L, Xu J. Emerging roles of keratinocytes in nociceptive transduction and regulation. Front Mol Neurosci 2022;15:982202.

Yamaoka S, Ito N, Ohka S, Kaneda S, Nakamura H, Agari T, et al. Involvement of the rabies virus phosphoprotein gene in neuroinvasiveness. J Virol 2013;87:12327–38.

Yang Y, Huang Y, Gnanadurai CW, Cao S, Liu X, Cui M, et al. The inability of wild-type rabies virus to activate dendritic cells is dependent on the glycoprotein and correlates with its low level of the de novo-synthesized leader RNA. J Virol 2015;89:2157–69.

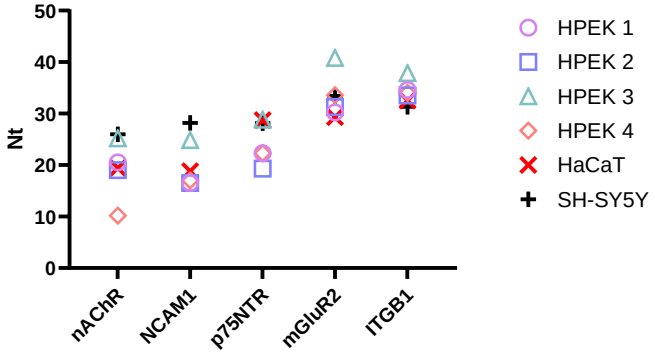

	nAChR	NCAM1	p75NTR	mGluR2	ITGB1	TBP
HPEK 1	32.6	36.6	30.8	22.9	18.5	26.5
HPEK 2	32.9	35.4	32.6	20.6	18.4	26.0
HPEK 3	32.5	32.9	28.9	16.9	19.9	28.9
HPEK 4	41.6	34.9	29.5	18.3	17.8	25.9
HaCaT	32.1	32.7	22.8	22.2	19.0	25.8
SH-SY5Y	28.1	25.9	25.9	20.7	22.8	27.1

Supplementary Figure S1. Expression of RABV entry receptors by primary keratinocytes, HaCaT, and SH-SY5Y cells. Expression levels were determined using RT-qPCR. Graph shows normalized threshold (denoted as Nt) values, calculated as Nt = 2Ct[TBP]-Ct[target]. Table shows raw Ct values. HPEK, human primary epidermal keratinocyte; RABV, rabies virus.

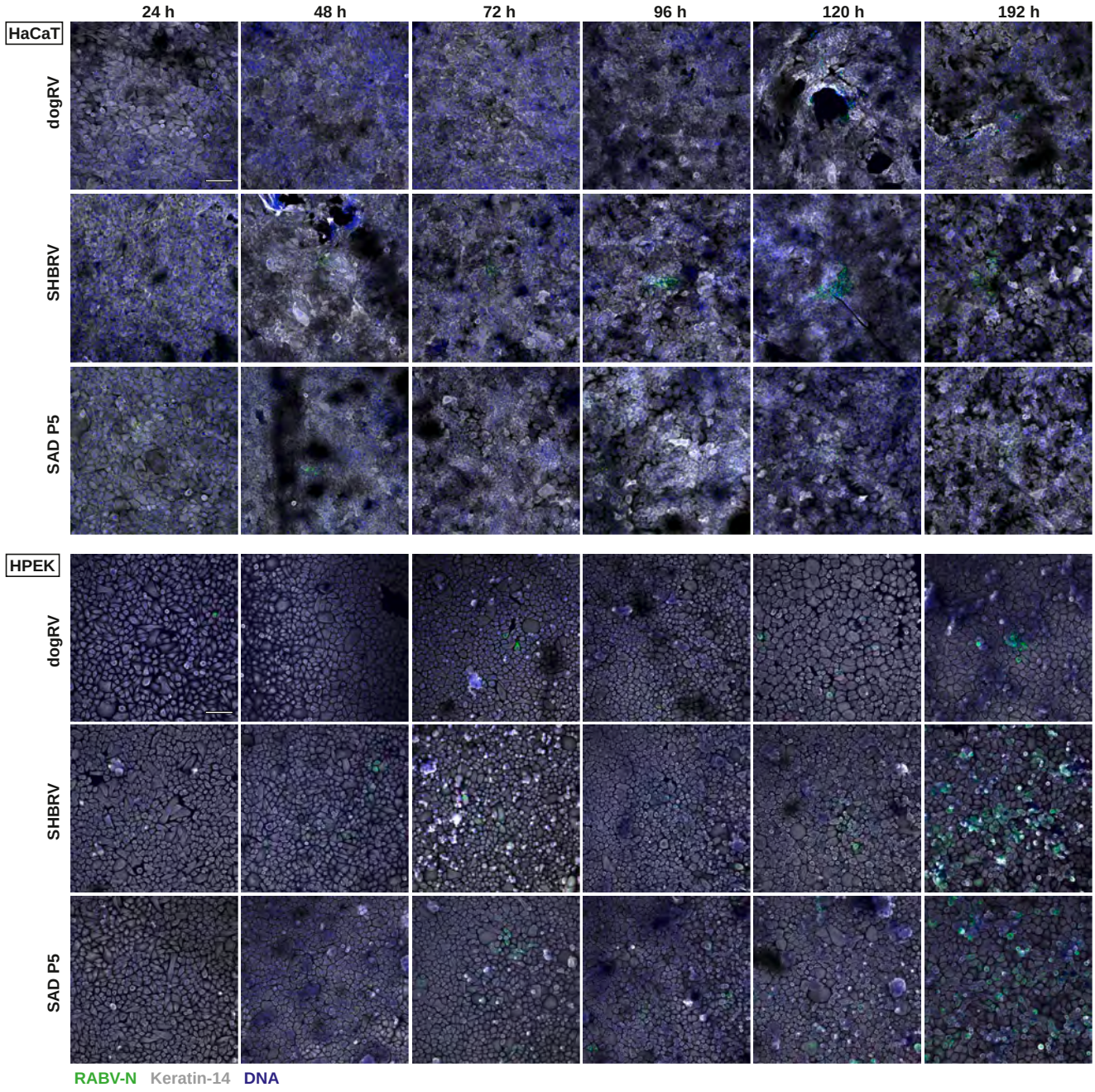

Supplementary Figure S2. Infection of keratinocytes over a time course of 24–192 hpi. HaCaT and HPEKs were infected with RABV strains dogRV, SHBRV, and SAD P5, at an MOI of 0.1, and cells were fixed every 24 hours. Visualization of infection using an anti–RABV-N antibody (green) was performed. Bar = 100 μm. dogRV, dog-related rabies virus; HPEK, human primary epidermal keratinocyte; hpi, hour after infection; MOI, multiplicity of infection; RABV, rabies virus; RABV-N, rabies virus nucleoprotein; SHBRV, silver-haired bat rabies virus.

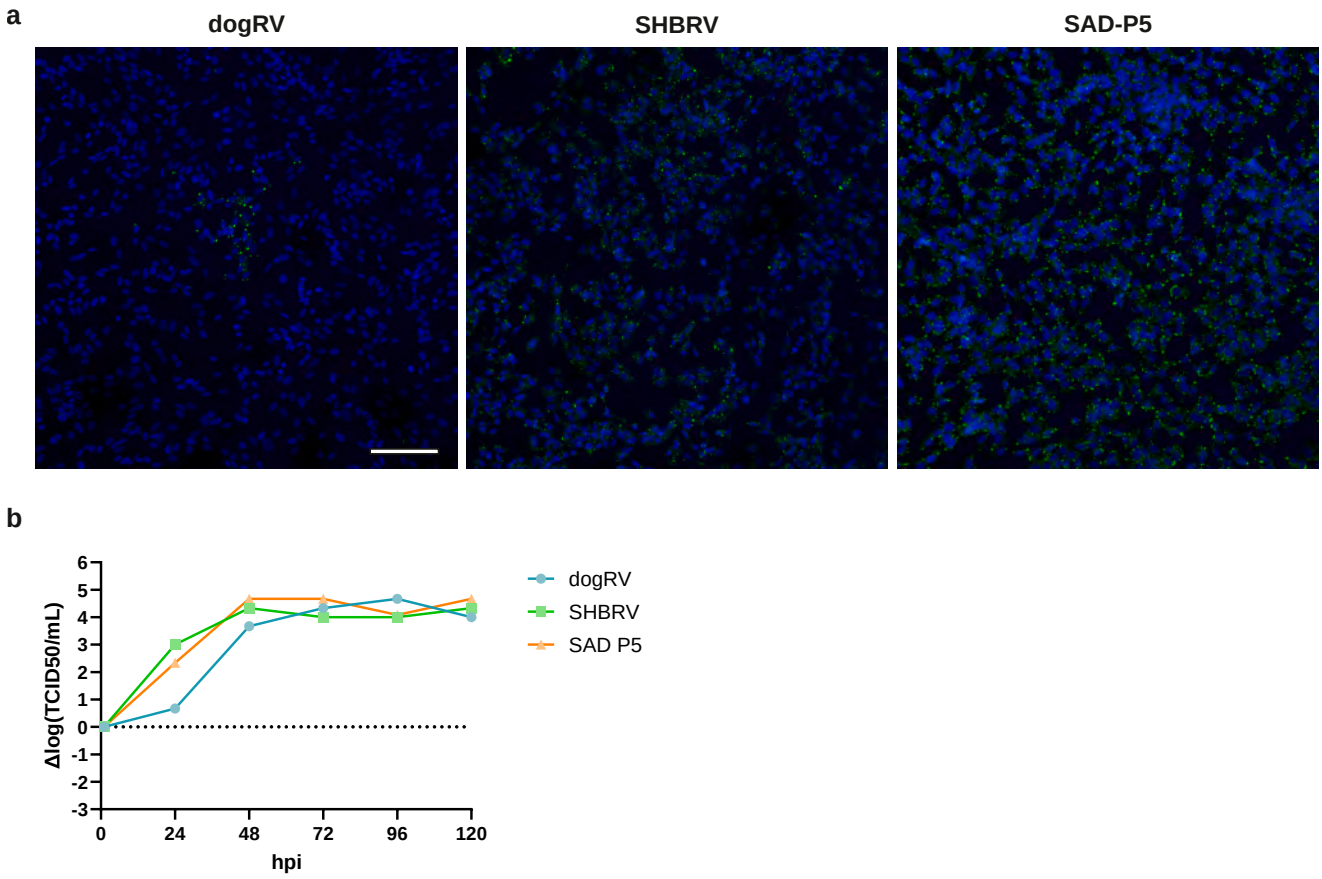

Supplementary Figure S3. Infection of SH-SY5Y cells with RABV. (**a**) SH-SY5Y cells were infected with RABV strains dogRV, SHBRV, and SAD P5 at an MOI of 0.01 and imaged at 72 hpi. Cells were stained for RABV-N protein (green), and nuclei were counterstained with Hoechst (blue). Bar = 100 μm. (**b**) Viral titers in culture supernatants of SH-SY5Y cells infected at MOI 0.1. Values are shown as Δlog(TCID50/ml), representing the increase or decrease in viral titers compared with 1 hpi. dogRV, dog-related rabies virus; hpi, hour after infection; MOI, multiplicity of infection; RABV, rabies virus; RABV-N, rabies virus nucleoprotein; SHBRV, silver-haired bat rabies virus.

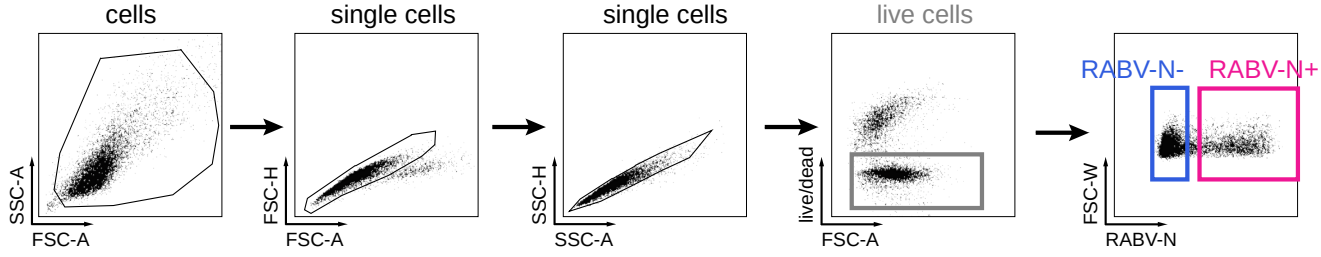

Supplementary Figure S4. Gating strategy for RABV-N+ and RABV-N− populations. Flow cytometry populations were gated on the basis of FSC and SSC area (-A), height (-H), and width (-W), viability stain, and intracellular RABV-N staining. Surface HLA-DR, HLA-ABC, ICAM-1, and PD-L1 expression was measured in the total live cell population (gray), the RABV-N− fraction (blue), and the RABV-N+ fraction (pink). FSC, forward scatter; RABV-N, rabies virus nucleoprotein; SSC, sideward scatter.

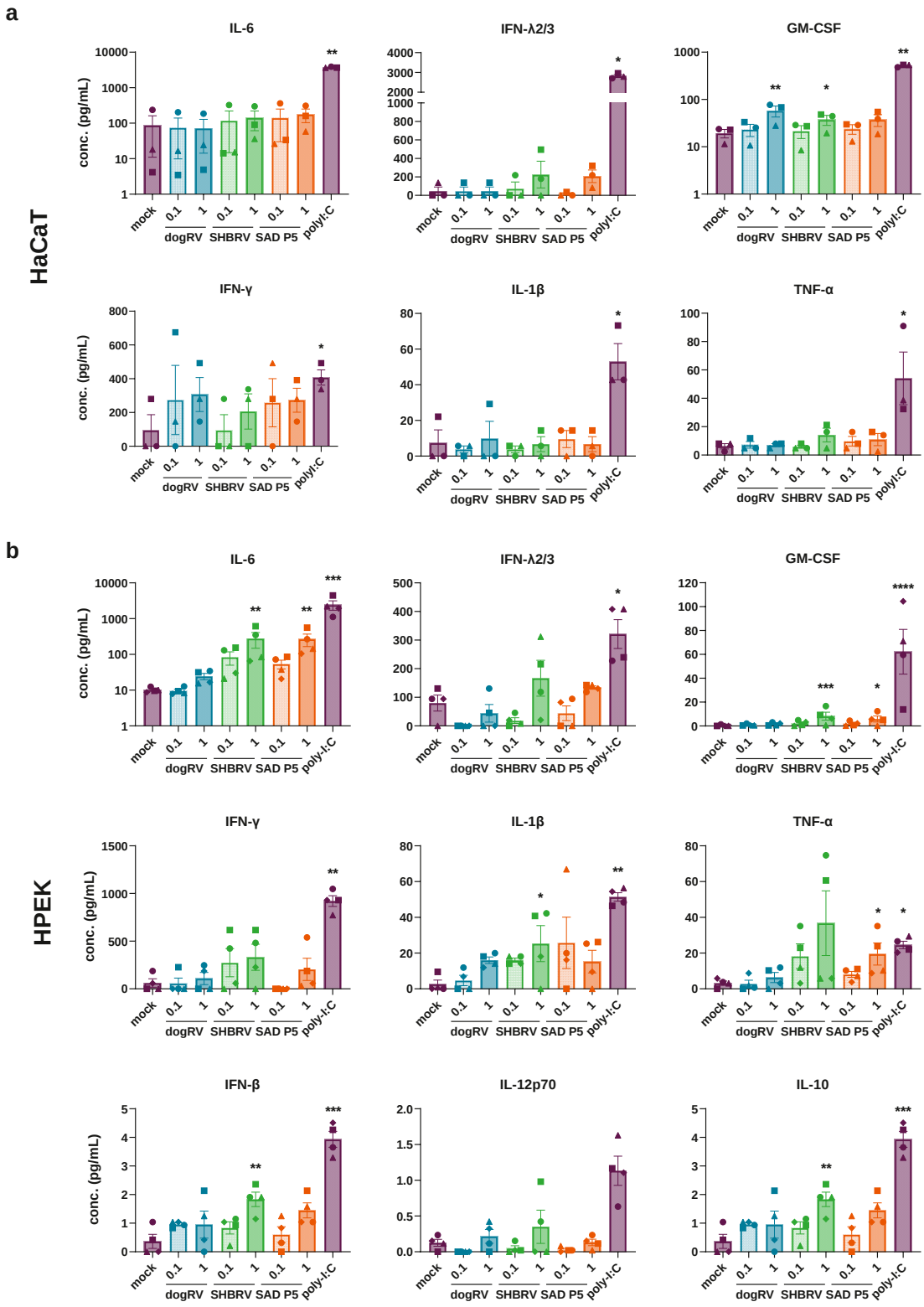

Supplementary Figure S5. Cytokine release of keratinocytes exposed to RABV. Keratinocytes were exposed to RABV strains dogRV, SHBRV, and SAD P5, at MOIs of 0.1 and 1. Supernatants were taken at 72 hpi, and cytokines were measured using a commercial multiplex bead-based assay. (**a**) Cytokine concentrations in supernatants of HaCaT cells. Cytokines IL-12p70, IFN-ß, and IL-10 were not detected in most samples and, therefore, excluded from analysis. (**b**) Cytokine concentrations in supernatants of HPEKs. Bars represent mean values ± SEM, and symbol shapes correspond to independent experiments (HaCaT, n = 3) or individual donors (HPEK, n = 4). Statistical significance was determined using Friedman test and Dunn's uncorrected multiple comparison test with the mock as control condition. ****$P \leq .0001$, ***$P \leq .001$, **$P \leq .01$, and *$P < .05$. dogRV, dog-related rabies virus; HPEK, human primary epidermal keratinocyte; hpi, hour after infection; MOI, multiplicity of infection; RABV, rabies virus; SHBRV, silver-haired bat rabies virus.

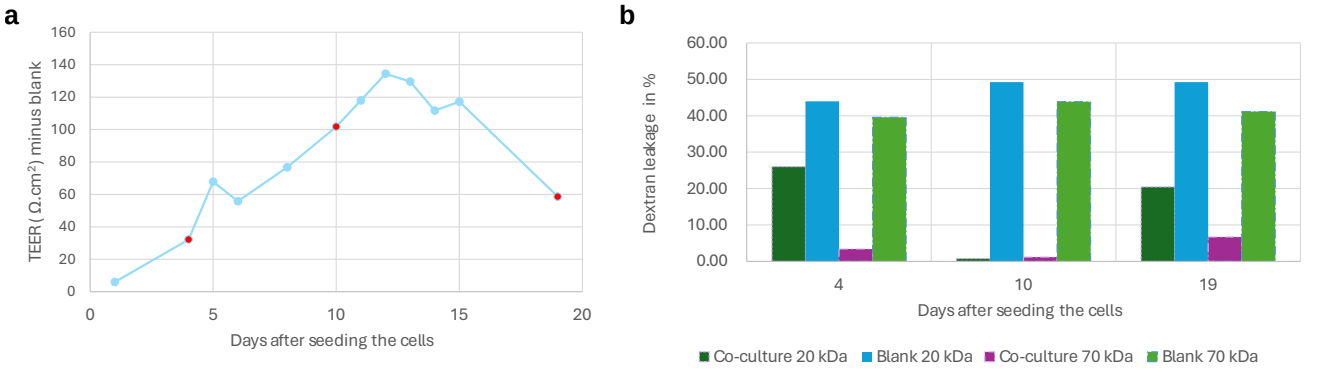

Supplementary Figure S6. Barrier permeability of the transwell coculture model. (**a**) TEER measurement of the coculture over time. Timepoints at which the dextran permeability was measured are indicated in red. (**b**) Leakage of 20 and 70 kDa fluorescent FITC dextran from the apical to the basolateral compartment within 24 hours at days 4, 10, and 19 after cell seeding. TEER, transepithelial electrical resistance.

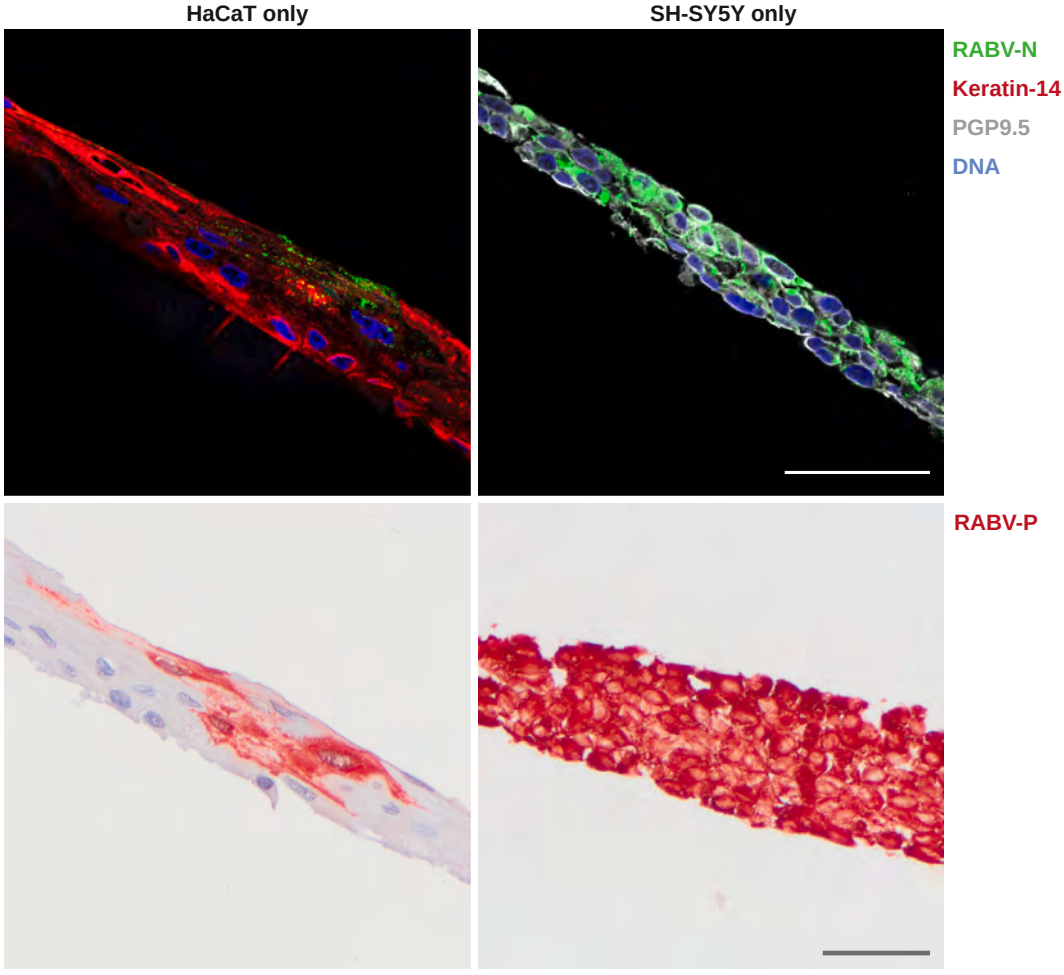

Supplementary Figure S7. Presence of RABV antigen in transwell monocultures. Transwell inserts with either HaCaT (left) or SH-SY5Y cells (right) only were infected with SHBRV at an MOI of 1 for 96 hours. Cross-sections were stained for immunofluorescence (top) with an anti–RABV-N antibody (green) or for immunohistochemistry (bottom) with an anti–RABV-P antibody (red). Bar = 50 μm. MOI, multiplicity of infection; RABV, rabies virus; RABV-N, rabies virus nucleoprotein; RABV-P, rabies virus phosphoprotein; SHBRV, silver-haired bat rabies virus.